Macromolecules

ARTICLE

pubs.acs.org/Macromolecules

Nonaffine Displacements in Flexible Polymer Networks

Anindita Basu,*[,†] Qi Wen,[‡] Xiaoming Mao,[†] T. C. Lubensky,[†] Paul A. Janmey,[‡,†] and A. G. Yodh[†]

[†]Department of Physics and Astronomy, University of Pennsylvania, Philadelphia, Pennsylvania 19104, United States

[‡]Institute for Medicine and Engineering, University of Pennsylvania, Philadelphia, Pennsylvania 19104, United States

Supporting Information

ABSTRACT: The validity of the affine assumption in model flexible polymer networks is explored. To this end, the displacements of fluorescent tracer beads embedded in polyacrylamide gels are quantified by confocal microscopy under shear deformation, and the deviations of these displacements from affine responses are recorded. Nonaffinity within the gels is quantified as a function of polymer chain density and cross-link concentration. Observations are compared with current theories of nonaffinity in random elastic media. We note that the mean-squared nonaffine deviation is proportional to the square of the applied strain in the linear elasticity regime, as per theoretical predictions. The measured degree of nonaffinity in the polyacrylamide gels suggests the presence of structural inhomogeneities which likely result from heterogeneous reaction kinetics during gel preparation. In addition, the macroscopic elasticity of the polyacrylamide gels is confirmed to behave in accordance with standard models of flexible polymer network elasticity.

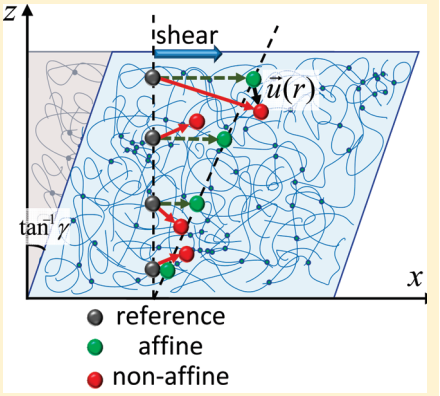

1. INTRODUCTION

Affine deformation is an essential assumption in the classical theory of elasticity. In the classical theory, deformation is assumed to be distributed homogeneously in the material so that strain is spatially constant at all length scales. The affine assumption permits elastic properties of cross-linked polymer networks to be readily derived from theories of rubber elasticity based on the entropy of a single polymer chain in the network. In practice, however, such affine deformations only occur in perfect crystals under very small deformation. In polymer networks, especially networks composed of semiflexible or rigid filaments, the microscopic network deformations should be nonaffine below a certain length scale.

Nonaffinity can arise from different sources. In near-ideal flexible polymer melts, deformations might be expected to be affine on length scales much larger than the average mesh size and nonaffine at lengths scales of the order of the mesh size or smaller.[1] Random thermal fluctuations of the cross-link junctions along with thermal undulations of the polymer chains may also lead to nonaffine behavior in polymer gels. Inhomogeneities introduced into the network microstructure during sample preparation can also introduce nonaffine responses; such inhomogeneities might be expected to be a function of reaction kinetics and other sample preparation parameters.[2]

Over the years, the connection between shear deformation and nonaffinity has been explored theoretically in a wide range of materials including rubber-like spatially homogeneous elastic media,[2] entangled or cross-linked polymer networks,[3−7] semiflexible polymer networks with rigid[8] and flexible cross-links,[9] stiff rod networks,[10] biopolymers,[11] amorphous systems,[12] and foams.[13] Indeed, it has been proposed that nonlinear elasticity in polymer networks has its origin in nonaffine responses.[1] In spite of continued interest in this problem and its fundamental importance, relatively little experimental quantification of the nonaffine phenomenon has been carried out in semiflexible biopolymer gels,[15,20] and we are not aware of any nonaffinity studies for the simple case of flexible polymers. Experiments along these lines should provide benchmarks for future understanding of the subject.

This paper describes an investigation of nonaffine shear deformations in a model flexible polymer gel: polyacrylamide gels with (bis)acrylamide cross-links. Polyacrylamide is well suited for the investigation because it is comparatively well-controlled, and its stiffness is tunable by the number of (bis)acrylamide cross-links. As part of this study, macroscopic rheological measurements are carried out to confirm the simple rubber-like elastic character of these networks. Then deformation fields in the gels under external shear stress are characterized by measuring the displacements of fluorescent beads entrapped in the gels. Bulk rheology and confocal microscopy are used in concert for the latter study. A nonaffine parameter, $\mathcal{A}$, is defined to quantify the degree of nonaffinity in the displacement field. $\mathcal{A}$ is measured as a function of bead size, polymer chain density, and cross-link density in the gels. We test simple predictions of a recently developed theory of nonaffinity in random elastic media[2] and obtain estimates for the fluctuations in elastic modulus of the gels from $\mathcal{A}$.

Received: November 24, 2010
Revised: January 26, 2011
Published: February 21, 2011

2. EXPERIMENT

2.1. Sample Preparation. The polyacrylamide (PA) gel is prepared by polymerizing acrylamide monomers and (bis)acrylamide (bis) cross-links in aqueous 50 mM HEPES buffer at pH = 8.2, using free-radical polymerization reaction initiated by 0.1% weight/weight (w/w) ammonium persulfate (APS) and 0.3% w/w *N,N,N′,N′*-tetramethylethylenediamine (TEMED). (Here the percent of X w/w equals the mass in grams of X per 100 g of solution.) Fluorescent polystyrene tracer beads are mixed into our solution at a concentration of 0.004% weight per volume (w/v), before the addition of bis cross-links. (Here the percent of X w/v equals the mass in grams of X dissolved/suspended in 100 mL of solvent.) Thus, a tracer bead concentration of 0.004% w/v is attained by dissolving 0.004 g of tracer beads in 100 mL of water. This procedure helps to distribute the beads uniformly throughout the polymer network. Internally labeled and carboxylate-modified fluorescent polystyrene microspheres of various diameters are used for this purpose, viz., 0.6 μm, 1 μm (Molecular Probes, Sunnyvale, CA), and 1.5 μm (Bangs laboratories Inc., Fishers, IN). Acrylamide (7.5%, 15% w/v) and (bis)acrylamide (0.03−0.12% w/v) concentrations are systematically changed to study the effects of polymer concentration, cross-link density, and mesh size on the polymer network rheology.

2.2. Rheology. Rheology measurements are performed using a stress-controlled Bohlin Gemini rheometer (Malvern Instruments, UK), with a cone and plate geometry of 4° cone angle and 20 mm diameter. Samples are prepared *in situ* so that good contact is routinely established between the sample surfaces and the rheometer plates to prevent slippage at high strains. The shear storage modulus (G') and loss modulus (G'') for each sample during the process of polymerization are monitored using low strain amplitude ($\gamma_0 = 0.01$) and low frequency ($f = 0.1$ Hz) oscillatory shear measurements. The polymerization reaction proceeds for ∼30 min, with the elastic and viscous moduli attaining steady-state values in less than 10 min. Care is taken to prevent solvent evaporation by sealing off the sample from the sides with a low density, low viscosity (∼50 mPa·s) silicone oil. The elastic and viscous moduli, G' and G'', respectively, for these gels are measured as functions of frequency, amplitude, and temperature. These measurements are intended to confirm that the gels behave in accordance with the existing theories of flexible polymer networks.[16] A set of control experiments are performed on the PA gels, with and without the tracer beads, to further confirm that macroscopic properties of the gels are not altered by the addition of the tracer beads.

2.3. Confocal Microscopy. Microscopic deformation of the PA gels under shear is studied by tracking tracer bead displacements in the sample using confocal microscopy. A VTeye confocal system (VisiTech International, UK) is used in conjunction with an inverted Eclipse TE200 microscope (Nikon Instruments) for this purpose. The lower plate of the rheometer is replaced by a home-built transparent sample holder and is mounted on the microscope to permit visualization of the samples under shear (Figure 1a).

A 60× water objective (NA = 1.2) is used to visualize the sample over a depth of 100 μm. 3D stacks map the entrapped tracer beads (70 μm × 70 μm × 60 μm) using the confocal setup with and without applied shear. The step size of the 3D stacks is varied from 100 to 200 nm for tracer bead sizes ranging from 600 nm to 1.5 μm. A wide range of shear strain, up to 50% amplitude, is applied.

The image stacks are processed using relatively standard Matlab routines, which determine the beads' positions with subpixel accuracy.[17,18] For each stress value, a set of two image stacks are taken, one with shear and one without. The 3D locations of beads in a gel without external shear stress are determined as $(x_{0i}y_{0i}z_{0i})$, for $i = 1, 2, ..., N$, where N is the number of tracked beads. The centroids of the corresponding N beads in the image stack under shear stress are measured too, as $(x_iy_iz_i)$; for convenience, the direction of shear is taken to be along the $\vec{x}$ axis in the figure. The displacements of tracer beads are then calculated from the tracking results

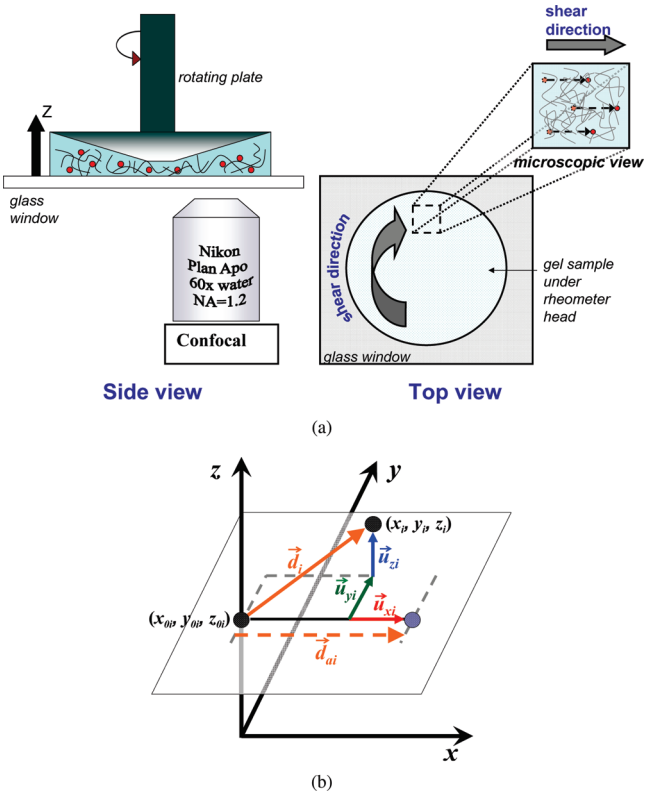

Figure 1. Experimental setup. (a) Experimental schematic. (b) Sketch of the nonaffine displacements of tracer beads. $(x_{0i}y_{0i}z_{0i})$ and $(x_iy_iz_i)$ mark the positions of a tracer bead without and under shear, respectively. Dashed arrow indicates affine displacement, $\vec{d}_{ai}$, of tracer bead in the direction of shear (x-axis). $\vec{d}_i$ is the measured displacement of the tracer bead. $\vec{u}_{xi}$, $\vec{u}_{yi}$, and $\vec{u}_{zi}$ indicate the nonaffine deviations along the x, y, and z axes, respectively. $\vec{u}_i = \vec{d}_{ai} - \vec{d}_i$ is the nonaffine deviation.

as $\vec{d}_i = (x_i - x_{0i}, y_i - y_{0i}, z_i - z_{0i})$. The system permits the displacements of tracer beads to be measured with a spatial resolution of 50 nm. On average, 30 beads are tracked in each 3D stack.

2.4. Nonaffine Parameter. A measure of the degree of nonaffinity is provided by the nonaffine parameter $\mathcal{A}$, which is defined in ref 2 as

$$\mathcal{A} = \frac{1}{N}\sum_{i=1}^{N} |\vec{u}_i|^2$$

Here $\vec{u}_i = \vec{d}_i - \vec{d}_{ai}$ is the deviation of the measured tracer-bead displacement, $\vec{d}_i$, from the affine displacement, $\vec{d}_{ai}$ (Figure 1b). This definition is similar to the definitions of nonaffine parameters used in a range of different systems, e.g., foams,[13] semiflexible networks,[9,15,20,43,44] etc.

For a perfect shear deformation along the x-axis, the affine displacement $\vec{d}_{ai}$ would be in the direction of shear only—the y and z components must be zero. We measure the resultant strains along all three component axes, γ_x, γ_y, and γ_z by fitting the x, y, and z components of d_i to linear functions of z_{0i}, as seen from a sample PA gel (7.5% acrylamide and 0.03% bis) under an applied strain of $\gamma = 0.3$ in Figure 2a. The real strain on the sample is determined as $\gamma = (\gamma_x^2 + \gamma_y^2 + \gamma_z^2)^{1/2}$. The x, y, and z components of the affine displacement vector, $\vec{d}_{ai}$, are then calculated as $z_{0i}\gamma_x$, $z_{0i}\gamma_y$, and $z_{0i}\gamma_z$. Note that the y and z components, both perpendicular to the direction of shear, do not vary as a function of z_i, resulting in γ_y and $\gamma_z \approx 0$. Figure 2b plots the distribution of nonaffine deviations, $\vec{u}_x$, $\vec{u}_y$, and $\vec{u}_z$, for the same sample gel, along the x-, y-, and z-axes, respectively, for the same strain of $\gamma = 0.3$ as seen in Figure 2a. $|\vec{u}_i|^2$

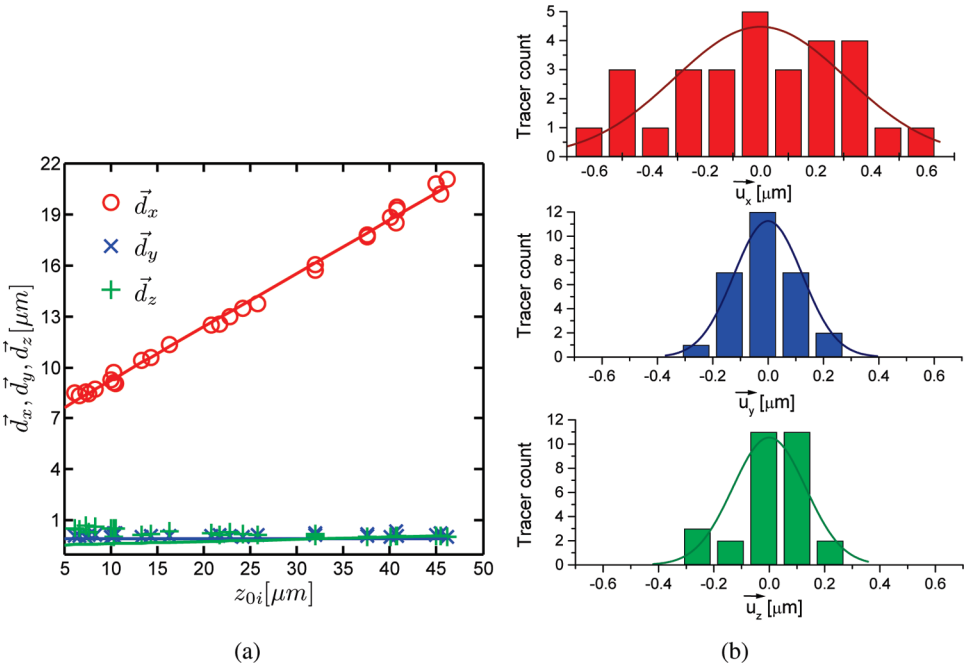

(a) (b)

Figure 2. (a) Experimentally measured displacements of tracer beads in the direction of shear, $\vec{d}_i$, that has been decomposed along x-axis (red circles), y-axis (blue crosses), and z-axis (green pluses) as a function of the distance, z_{0i}, from the fixed lower plate of the rheometer. This sample is 7.5% acrylamide and 0.03% bis PA gel. The solid lines give the strains, γ_x, γ_y, and γ_z obtained from their linear fits. Note that γ_y and γ_z are ≈0. (b) Distribution of nonaffine deviations of tracer beads for the same sample PA gel shown in (a) at $\gamma = 0.3$, decomposed along the x-, y-, and z-axes. The measurements are normally distributed around the *affine* displacement position, as indicated by the solid curves.

is calculated as $(x_i - x_{0i} - \gamma_x z_{0i})^2 + (y_i - y_{0i} - \gamma_y z_{0i})^2 + (z_i - z_{0i} - \gamma_z z_{0i})^2$.

The nonaffine parameter, $\mathcal{A}$, is then defined in terms of these variables as

$$\mathcal{A} = \frac{1}{N}\sum_{i=1}^{N}[(x_i - x_{0i} - \gamma_x z_{0i})^2 + (y_i - y_{0i} - \gamma_y z_{0i})^2 + (z_i - z_{0i} - \gamma_z z_{0i})^2] \quad (1)$$

3. RESULTS

3.1. Bulk Rheology Measurements. The PA gels used in our experiments are solidlike materials with G' ranging from 7.7×10^2 to 1.5×10^4 Pa, 2 to 3 orders of magnitude larger than the G''. In Figure 3a, G' and G'' of a gel made of 7.5% acrylamide and 0.06% (bis)acrylamide are plotted as functions of the amplitude of the oscillatory shear strain at oscillation frequency, $f = 0.1$ Hz. G' is ∼100 times larger than G''. Moreover, both G' and G'' are independent of the applied shear strain for strains up $\gamma = 0.5$, confirming the linear elastic response of PA gels. The frequency response of PA gels is characterized by measuring G' and G'' at oscillatory strains with amplitude $\gamma_0 = 0.01$ and frequency ranging from 0.1 to 100 Hz. Within this frequency range, G' remains constant, and G'' increases with increasing frequency (data not shown).

The elastic moduli of our PA gels vary linearly with (bis)acrylamide concentration and sample temperature. Cross-link and monomer concentration trends are shown in Figure 3b. Notice, when the (bis)acrylamide concentration increases from 0.03% to 0.12%, G' for gels with 7.5% acrylamide increases linearly from 7.7×10^2 Pa to 4.9×10^3 Pa. Similarly, G' for 15% acrylamide PA gels increases from 1.6×10^3 Pa at 0.005% bis to 1.5×10^4 Pa at 0.05% bis concentration. We also investigated the temperature dependence of the network elasticity within the attainable temperature range of the rheometer, i.e., 5 °C < T < 90 °C. In Figure 3c, we show that G' from the gel made of 7.5% acrylamide and 0.09% (bis)acrylamide increases linearly with sample temperature. This linear dependence of G' on cross-link concentration and sample temperature follows the predictions of classical rubber elasticity theory. Note, the slope of the linear fit of G' as a function of cross-link concentration for the 7.5% acrylamide is lower than that of 15% acrylamide PA gels. We suggest that some bis molecules form efficient cross-links and others do not and that this difference in the slope of G' versus cross-link concentration for 7.5% and 15% acrylamide are due to the difference in effectiveness of the bis molecules in forming efficient cross-links, which increases with increasing monomer concentration. We discuss these effects further in section 4.1.

3.2. Nonaffine Parameter, $\mathcal{A}$ Scales as the Square of the Applied Strain. Confocal microscopy is used to visualize and record the displacements of the fluorescent tracer beads entrapped within a (70 μm × 70 μm × 60 μm) volume in the PA gel. Since the tracer beads' size of ∼1 μm is much larger than the average mesh size of the PA gel, free Brownian motion is suppressed. Within this small volume, located ∼1 cm from the axis of rotation, the macroscopic shear strain applied to the beads can be approximated as unidirectional.

In Figure 2a, bead displacements along the x, y, and z axis, are plotted as a function of z_{0i}, the distance between the beads and the bottom surface. The displacements along the direction of shear, viz., the x-axis, increase linearly with z_{0i}, as expected from macroscopic shear deformation. Fitting d_x to a linear function of z_{0i} yields the strain $\gamma_x \approx \gamma$. d_y and d_z, both perpendicular to the shear direction, are independent of z_{0i} as shown in Figure 2a. Also notice from Figure 2b that the nonaffine displacements along

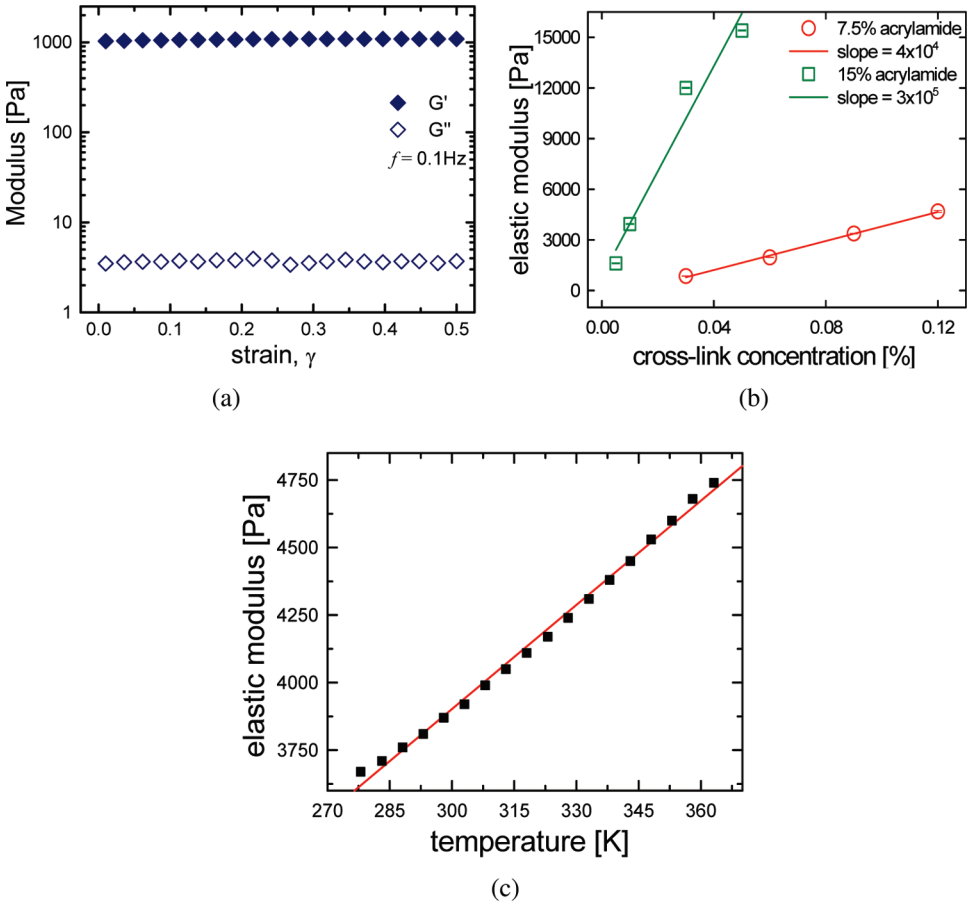

Figure 3. Rheology of polyacrylamide gels. (a) G' of sample PA gel is 2 orders of magnitude larger than the G'', and these values remain constant over a wide range of applied strain. Data are shown for a gel with 7.5% acrylamide at 0.03% bis(acrylamide) cross-link concentration, at an oscillatory frequency of 0.1 Hz. (b) G' of 7.5% and 15% polyacrylamide gels as a function of cross-link concentrations. Error bars denote standard deviations which are less than 2% of the mean elastic moduli. The solid lines indicate linear fits to the data. Note that the overall moduli of the gels with 7.5% acrylamide are significantly lower than that of 15% acrylamide for comparable cross-link density. (c) G' as a function of temperature (red line is the linear fit). Data are shown for a PA gel with 7.5% acrylamide with 0.09% bis(acrylamide).

each axis, viz., $\vec{u}_x$, $\vec{u}_y$, and $\vec{u}_z$, are much larger than the resolution of our system in the xy-plane (∼50 nm) and comparable to that along the z-axis (∼80 nm) and are normally distributed with mean value zero, i.e., distributed around the affine displacement positions. These uncertainties in tracking lead to a noise floor in $\mathscr{A} \sim 0.007\ \mu m^2$.

The nonaffine parameter $\mathscr{A}$ is readily computed from the measured bead displacements using eq 1 for PA gels (7.5% and 15% acrylamide and a range of (bis)acrylamide concentrations). In Figure 4a, $\mathscr{A}$ increases with applied strain γ and clearly scales as γ^2.

In ref 2, DiDonna and Lubensky developed a perturbation theory for nonaffine deformations in solids with random, spatially inhomogeneous elastic moduli. They characterized the nonaffine deformations using the nonaffinity correlation function

$$\mathscr{G}_{ij}(x,x') = \langle \vec{u}_i(x)\ \vec{u}_j(x') \rangle \qquad (2)$$

where $u(x)$ is the nonaffine displacement field, i and j are Cartesian indices, and $\langle \cdots \rangle$ represents the average over randomness in the elastic moduli (i.e., a disorder average). Because the disorder averaged quantities are translationally and rotationally invariant in the gel we consider, the correlation function only depends on the distance $|x - x'|$, and thus it is characterized by the Fourier transform $\mathscr{G}(q) \equiv \int d(x-x').\mathscr{G}_{ii}(x,x')e^{-iq\cdot(x-x')}$. In ref 2 it is proved that this correlation function is related to the correlation function of the inhomogeneous elastic modulus K as

$$\mathscr{G}(q) \sim \frac{\gamma^2 \Delta^K(q)}{q^2 K^2} \qquad (3)$$

where K is the disorder averaged elastic modulus and $\Delta^K(q)$ is the Fourier transform of the spatial correlation function of the elastic modulus K.

In this theory, the zeroth-order problem concerns elastic deformations in a homogeneous media of elastic modulus K, and the randomness in K is treated as a perturbation from this homogeneous state. To first order, the driving forces of the nonaffine deformations are thus proportional to the zeroth-order deformations, which are proportional to γ. Therefore, to first order in perturbation theory, $\mathscr{G}(q)$, is proportional to γ^2.

We show in section 3 of the Supporting Information that the two-point nonaffinity correlation function, $\mathscr{G}_{ij}(x,x')$ decays as $1/|x - x'|$, where $(x - x')$ is the separation between tracer beads in the PA gel samples.[2] For typical tracer-bead concentrations used in our experiments, the smallest separation between tracer beads is of the order of several micrometers, for which the $\mathscr{G}_{ij}(x,x')$ falls

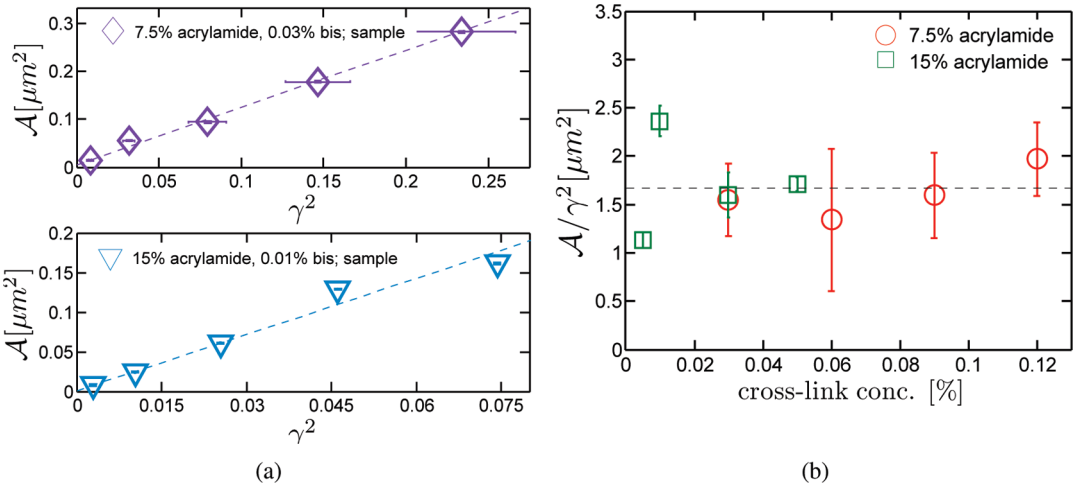

Figure 4. (a) The nonaffine parameter scales as the square of the external strain, as seen for sample polyacrylamide gels at 7.5% acrylamide and 0.03% bis (top) and 15% acrylamide and 0.01% bis (bottom). The dashed lines give best linear fits to the data. Error bars represent standard deviation of measurements of strain and nonaffinity, the latter being smaller than symbol size. (b) Strain-normalized nonaffine parameter, $\mathcal{A}/\gamma^2$, for sample PA gels at 7.5% and 15% acrylamide are plotted at varying bis concentrations. The data points and error bars represent the average value and standard error of measurements from different samples prepared in the same manner. The dashed line indicates the average $\mathcal{A}/\gamma^2$ calculated from all data points in the figure.

below our experimental noise floor. Thus, our tracer-bead concentration does not permit us to perform two-point nonaffinity correlation analysis at any meaningful length scales (e.g., length scales of inhomogeneities in PA gels, mesh size, etc., which are all $\lesssim$200 nm).

The nonaffine parameter $\mathcal{A}$ defined in the present experiment corresponds to $\mathcal{G}_{ii}(x,x)$

$$\mathcal{A} = \mathcal{G}_{ii}(x,x) = \int \frac{d^3q}{(2\pi)^3}\,\mathcal{G}(q) \sim \int \frac{d^3q}{(2\pi)^3}\,\frac{\gamma^2\Delta^K(q)}{q^2K^2} \quad (4)$$

It is clear from this equation that $\mathcal{A} \propto \gamma^2$. In our experiment the relation $\mathcal{A} \propto \gamma^2$ is verified, as shown in Figure 4a. This fairly robust relation has also been found in nonaffine correlation functions of, for example, flexible polymer networks[19] and semiflexible polymer networks at small strain.[20,21]

The quantity $\mathcal{A}/\gamma^2$, which is independent of strain γ, provides a good measure of the degree of nonaffinity of the sample. We shall refer to this quantity, $\mathcal{A}/\gamma^2$, as the strain-normalized nonaffine parameter. $\mathcal{A}/\gamma^2$ is calculated for each sample as follows: For a particular strain, $\mathcal{A}$ is calculated by averaging the square of the nonaffine displacements, $\vec{u}_i^{\,2}$, for all tracer beads in the sample; typically, we carried out multiple shear measurements at the same strain (see section 4.3), and the displacement data from all particles in all repeated shear measurements were averaged together to derive the mean $\mathcal{A}$ and its standard deviation. The resultant $\mathcal{A}/\gamma^2$ data were then fit to a linear function. The slope of the linear fit gives $\mathcal{A}/\gamma^2$ for the sample; the intercept from the fitting is comparable to the noise floor of the measurements in $\mathcal{A}$. Standard deviations for the slopes were also derived. We use this parameter, $\mathcal{A}/\gamma^2$, which represents an intrinsic material property, for comparisons among samples prepared at different times or under different conditions.

The $\mathcal{A}/\gamma^2$ value calculated for each sample along with its constituent acrylamide and bis concentration is listed in Table 2 in the Supporting Information. Figure 4b plots the mean and standard error of the strain-normalized nonaffinity parameter, $\mathcal{A}/\gamma^2$, for PA gel samples at various monomer (viz., 7.5% and 15% acrylamide, w/v) and cross-link (between 0.005% and 0.12% (bis)acrylamide, w/v) concentrations. The large error bars in the $\mathcal{A}/\gamma^2$ values for the 7.5% acrylamide samples at different bis concentration (standard deviation ~38%) arises primarily from sample-to-sample variations associated with gels polymerized under (ostensibly) identical experimental conditions. The error bars for the 15% acrylamide samples are much smaller than the 7.5% samples because data in the former case were extracted from a single sample polymerized at the given acrylamide and bis concentration. Within this relatively large range of values, the strain-normalized nonaffinity measure does not appear to vary significantly as a function of either the density of polymer chains or the network mesh size and is evenly distributed around the mean $\mathcal{A}/\gamma^2$ calculated over the entire range of PA gels sampled in our experiments. This mean value is indicated by the dashed line in Figure 4b. The average values of $\mathcal{A}/\gamma^2$ obtained for different monomer concentrations along with their respective standard deviation and standard error of each group of measurements are summarized in Table 1. We also used an alternative approach for calculating the mean $\mathcal{A}/\gamma^2$ in section 4 of the Supporting Information; this alternative approach treated all beads across all samples equally. The results obtained by this alternative method were essentially same as the results above. Perhaps not surprisingly, we will propose below that this measured nonaffinity is largely dominated by inhomogeneities formed during synthesis of the PA gels, rather than being dictated by the thermal fluctuations of the polymer cross-links.

Table 1. Summary of $\mathcal{A}/\gamma^2$ at Different Acrylamide Concentrations

monomer concn	$\mathcal{A}/\gamma^2$	std dev	std err
7.5%	1.65	±0.63	±0.21
15%	1.70	±0.51	±0.25
all samples	1.67	±0.57	±0.16

4. DISCUSSION

4.1. Effectiveness of Cross-Links. The measured G' of polyacrylamide gels generally follows predictions of standard

theories of rubber elasticity, i.e., $G' = 2\nu N k_B T$, where N is the number density of cross-links, k_B represents the Boltzmann constant, T represents temperature, and ν is the efficacy of cross-link.[16] Note the additional multiplicative factor of 2, which arises because (bis)acrylamide is a tetrafunctional cross-link. $\nu = 1$ implies that all cross-links are effective; i.e., the polymer strands attached to each cross-link are a part of the homogeneous network. Any unproductive reaction of bis(acrylamide) or inhomogeneity in the network, for example if one of the four polymer strands connected to a cross-link is a dangling chain which does not contribute to the elasticity of the polymer network, leads to $\nu < 1$.[14,16,22] Taking the molecular weight of a (bis)acrylamide as 154, the elasticity of a polyacrylamide gel at room temperature can be rewritten as $G' = 33.2 \times 10^4 \nu c$ measured in pascals, where c is the percentage concentration of (bis)acrylamide. In Figure 3b, we see that G' is equal to $4.0 \times 10^4 c$ Pa for polyacrylamide gels with 7.5% acrylamide, and $3.0 \times 10^5 c$ Pa for 15% acrylamide. Hence, $\nu = 0.12$ for the 7.5% and $\nu = 0.9$ for the 15% PA gels. The higher value of ν for 15% acrylamide PA gels is due to the higher polymer chain density in this system, suggesting that there is a higher probability for a bis molecule to find an acrylamide polymer chain in its neighborhood that would result in an effective cross-link.

Note, this scenario is over-simplified; ν does not keep increasing indefinitely with increasing polymer chain concentration but levels off as the semidilute limit for acrylamide chains is reached. The elastic modulus is also strongly affected by the amount of bis present, an excess of which may change the polymer solubility from good to theta solvent and the effective persistence length of the acrylamide chains,[23] and may even lead to macroscopic syneresis for sufficiently large concentrations of bis.[24] Thus, the relative concentrations of acrylamide and bis may have profound effect on the bulk modulus of PA gels, where instead of a linear scaling of the elastic modulus with the bis concentration, as seen in our samples (Figure 3b), the elastic modulus could level off[25] due to microphase separation in the gels. The roles of bis and acrylamide not only are limited to macroscopic elastic modulus but also have a significant impact on the microscopic nonaffinity of PA gels, as we note in the following section.

4.2. Elastic Inhomogeneities in Polyacrylamide Gels. The value of $\mathcal{A}/\gamma^2$ characterizes the inhomogeneities in the elasticity of the material. In this section we analyze two possible scenarios that give rise to randomness in elastic modulus K (i.e., randomness in the shear modulus G' of PA gels) and thus generate nonaffine responses in polyacrylamide gels. We then compare the predicted nonaffinity in these two scenarios with experimental results.

In the first scenario, the gel is assumed to be nearly ideal. The inhomogeneity is assumed to be produced by the intrinsic randomness in the network geometry arising from thermal fluctuations frozen into the PA gel at the moment of gelation; in this case, the smallest length scale characterizing the inhomogeneity would be the mesh size of the network, and the inhomogeneities cannot be reduced by improving the synthesis process. In the second scenario, "nonthermal" inhomogeneities are assumed to be introduced during the sample preparation process. For example, this effect could arise if the cross-links are not homogeneously distributed; in this second case, elastic inhomogeneities could be present at length scales much larger than the network mesh size.

The elastic modulus correlation function Δ^K in the first scenario can be modeled as

$$\Delta^K(x) = (\delta G')^2 \xi_e^3 \delta(x) \quad (5)$$

where $(\delta G')^2$ is the variance of the local shear modulus G', $\delta(x)$ is the Dirac delta function, and ξ_e is the characteristic mesh size of the network. In this scenario the gelation process is nearly ideal, and the only randomness comes from the frozen thermal fluctuations in the liquid at the moment of gelation. Thus, the correlation of the elastic modulus is characterized by the only length scale in the system, the mesh size ξ_e, which we also take to be the short-distance cutoff of the system because the picture of continuous elasticity breaks down below this length scale. Thus, the elastic modulus correlations at this scale are characterized by a Dirac delta-function in eq 4. The Fourier transform of Δ^K is then

$$\Delta^K(q) = (\delta G')^2 \xi_e^3 \quad (6)$$

We plug this correlation function back into eq 4 to calculate $\mathcal{A}$. To evaluate the integral, one has to set a small length scale cutoff, which is ξ as we discussed. Below this length scale the polymer network structure cannot be coarse-grained, and one cannot characterize the properties using continuous elasticity.

We obtain the nonaffine parameter $\mathcal{A}$ from the integral (ignoring unimportant $O(1)$ constant prefactor):

$$\mathcal{A} \sim \left(\frac{\delta G'}{G'}\right)^2 \gamma^2 \xi_e^2 \quad (7)$$

The experimentally measured $\mathcal{A}$ is plotted as a function of γ^2 at two different monomer and cross-link concentrations in Figure 4a. Both results are consistent with the theoretical prediction that $\mathcal{A}$ is proportional to γ^2. However, the magnitude of $\mathcal{A}/\gamma^2$ is of the order of 1 μm^2. Since the mesh size is expected to be of order 10 nm, we obtain $\delta G'/G' \sim O(10^2)$ from eq 7 and our measurements of $\mathcal{A}/\gamma^2$. This value is too large for a nearly ideal "thermal" gel. In a nearly ideal gel, the inhomogeneities in network geometry and thus the elasticity come purely from thermal fluctuations at the moment of gelation; thus, both $\delta G'$ and G' are of order $k_B T$ times the cross-link number density, so one should expect $\delta G'/G' \sim O(1)$. Furthermore, in this scenario $\mathcal{A}$ should be related to the concentration of cross-links c as $\mathcal{A} \propto \xi_e^2 \propto c^{-2/3}$ (because $\xi_e \propto c^{-1/3}$), but this behavior is not seen in Figure 4b, in which $\mathcal{A}/\gamma^2$ is essentially a constant (albeit with a wide scatter).

Other length scales in the gel will not significantly affect this analysis. The persistence length of the polymer chain is even smaller than the mesh size, the small length cutoff of the analysis, and thus will not affect the result. The size of the tracer bead, although on the scale of 1 μm and relevant to the problem, only weakly changes the value of $\mathcal{A}$, as we discuss in section 4.4 and section 2 of the Supporting Information.

The discrepancy between the value of $\delta G'/G'$ suggested by the experiment and the theoretical value of nearly ideal "thermal" gel suggests that our second scenario may be more realistic for these systems. In the second scenario, "nonthermal" inhomogeneities in the distribution of the (bis)acrylamide (cross-link) during the process of polymerization are assumed to exist. These inhomogeneities are frozen in at polymerization, and their contribution to the inhomogeneous elasticity in the resulting PA gel dominates over the contributions of thermal fluctuations at gelation described in the first scenario because these "nonthermal" inhomogeneities exhibit greater variance and longer correlation length, as we discuss below. These types of heterogeneities have

been recognized previously in the literature.[23,24,26−38] Briefly, because the hydrophobicity of polymerized (bis)acrylamide is higher than the polyacrylamide chains, the hydrophobic cross-links have a tendency to aggregate during the sample preparation.[24,39] This effect can generate an inhomogeneous spatial distribution of cross-links at length scales longer than the mesh size.

Thus, in the second scenario, regions with high shear modulus and regions with low shear modulus form in the polyacrylamide network as a result of the inhomogeneous distribution of cross-links frozen in during the process of sample preparation. We define the length scale ξ_G to characterize the size of this inhomogeneity. The resultant inhomogeneity in the shear modulus may then be characterized by a Gaussian correlation function

$$\Delta^K(r) = (\delta G')^2 e^{-r^2/2\xi_G} \quad (8)$$

We then plug this correlation function it back into eq 4. The integral is convergent due to the finite range of this correlation function, i.e., so the short length scale cutoff is not needed in this scenario. The resulting nonaffine parameter is given by

$$\mathcal{A} \sim \left(\frac{\delta G'}{G'}\right)^2 \gamma^2 {\xi_G}^2 \quad (9)$$

For a careful derivation of this relation with the exact value of the prefactor, see section 1 of the Supporting Information.

In fact, considerable effort has been expended over the years to characterize inhomogeneities inherent to PA gels. Starting with the pioneering work of Richards and Temple (1971),[28] various experimental techniques, viz., gel-swelling and permeability studies,[24,32,33] small-angle X-ray[23,24,26] and neutron scattering,[23,27] quasi-elastic light scattering,[23,35,38] dynamic light scattering,[24,37] UV−vis[34] and IR spectroscopy,[31] NMR spectroscopy,[30,31] and electron micrographs,[29] have been used to quantify the nature and size of inhomogeneities created in PA gels. Some of these ideas have been considered in the context of gel elastic properties,[36] as well as under varying acrylamide and bis concentration, and different polymerization reaction conditions. The ratio of monomer to cross-link concentrations, which determines the relative wettability of acrylamide and bis clusters during the polymerization process, as well as the reaction kinetics, all affect the formation of dense, heterogeneous clusters of highly cross-linked polymers interspersed with patches of sparsely cross-linked polymer chains. The size of these spatial inhomogeneties embedded in the more uniform gel matrix has been reported to vary widely from a few nanometers to as much as half a micrometer, with homogeneous regions of comparable length scale in between.

One may substitute the inhomogeneity correlation length, ξ_G, with the size of the spatial inhomogeneities reported in the aforementioned references. From the literature we find that 5 nm $\lesssim \xi_G \lesssim$ 500 nm, which gives corresponding range of inhomogeneity magnitude of $3 \lesssim \delta G'/G' \lesssim 300$ for PA gels over a wide range of monomer and cross-link concentrations. For PA gels synthesized under similar preparation conditions as in our experiment, the length scale of inhomogeneities has been measured using a nanoindentation method, leading to $\xi_G \lesssim$ 200 nm,[40] from which we obtain $\delta G'/G' \lesssim 7$.

4.3. Repeated Shear Measurements. As part of this study, we explored the effects of cycled measurements on $\mathcal{A}$ in the same sample. By repeatedly shearing and unshearing a PA gel sample at the same strain, we determined the distribution of $\mathcal{A}$ for the same set of particles within a single sample. The resultant variation of $\mathcal{A}$ is not insignificant, though it is considerably less than sample-to-sample error.

To demonstrate this effect, a PA gel sample is synthesized at 7.5% acrylamide and 0.06% bis with 1 μm tracer beads embedded in it. The gel is sheared repeatedly to a strain of 0.2, and $\mathcal{A}$ is measured each time as shown in Figure 5a. Error bars reflect the systematic error in our measurements. The tracer beads relax back roughly to their original (unsheared) positions once the strain is released. The variation in $\mathcal{A}$ suggests that some local rearrangement of the polymer network neighborhood occurs after/during each cycle, perhaps because of the presence of compliant chain entanglements or reorganization of the gel-bead interface. These rearrangements permit the tracer beads to explore and experience slightly different local environments every time the sample undergoes a shear transformation. Nonaffinity was slightly different after each shear event. The measured standard deviation of $\mathcal{A}/\gamma^2$ (∼8%) for repetitive shear in the sample is much smaller, however, than that measured for different gels prepared under apparently identical experimental conditions.

With respect to nonaffinity variation with repeated cyling, we have explored this phenomenon under different strains as well as for different polymer gel concentrations. It appears that the randomness persists even when a sample gel is sheared repeatedly 30 times. The variation in nonaffinity parameter appears to be random, independent of the number of times the gel is sheared. Chain entanglements, dangling ends, etc., could contribute to this randomness in the measured nonaffinity,[22] and one cannot rule out the possibility that the local environment of the tracer microbeads is subtly distorted due to polymer depletion or adsorption, which might cause more or less slippage or sticking of the tracer beads to the surrounding gel matrix under shear.[40,41] We use this repeated shear technique to calculate the systematic error in our measurements to be ∼8% and use this value as the lower bound for all error estimations shown in Figure 4b.

4.4. Tracer-Bead Size Dependence. We also explored the effects of the size of the tracer beads on the magnitude of the nonaffine parameter, $\mathcal{A}$, using tracer beads of three different sizes, viz., 0.6, 1, and 1.5 μm. The different-sized beads are fluorescently labeled such that they are uniquely excited by three different wavelengths of the confocal scanning beam, viz., 488, 568, and 640 nm, respectively. We disperse these three different-sized beads in a sample PA gel and image them using three different wavelength excitation beams in succession during a particular shear event. We see that, for the range of bead sizes used in our experiment, the magnitude of $\mathcal{A}$ remains within the range indicated in Table 1 for 7.5% acrylamide PA gels. We also note that there is a functional dependence on tracer bead size of the average value of $\mathcal{A}$ measured from repeated shear events. Figure 5b plots the average $\mathcal{A}$ from 11 repeated shear events at $\gamma = 0.3$ for a PA gel at 7.5% acrylamide and 0.06% bis as a function of bead size. We see that the average $\mathcal{A}$ decreases with an increase in the diameter of tracer beads. $\mathcal{A}$ can be fit to a linear function of tracer bead size, with a slope of $\sim -0.11 \pm 0.001$ μm^2 and an intercept of $\sim 0.27 \pm 0.002$, as shown. When fit to an inverse function of tracer bead diameter, we obtain a prefactor of 0.09 ± 0.025 μm^3 and an intercept of 0.06 ± 0.031 μm^2, also shown in the figure.

Essentially all of the theoretical analysis presented in this paper thus far employed the simplifying assumption that we can treat the tracer beads as point objects that probe local nonaffine deformations. However, the size of the tracer bead is comparable to the correlation length ξ_G of the random elastic modulus.

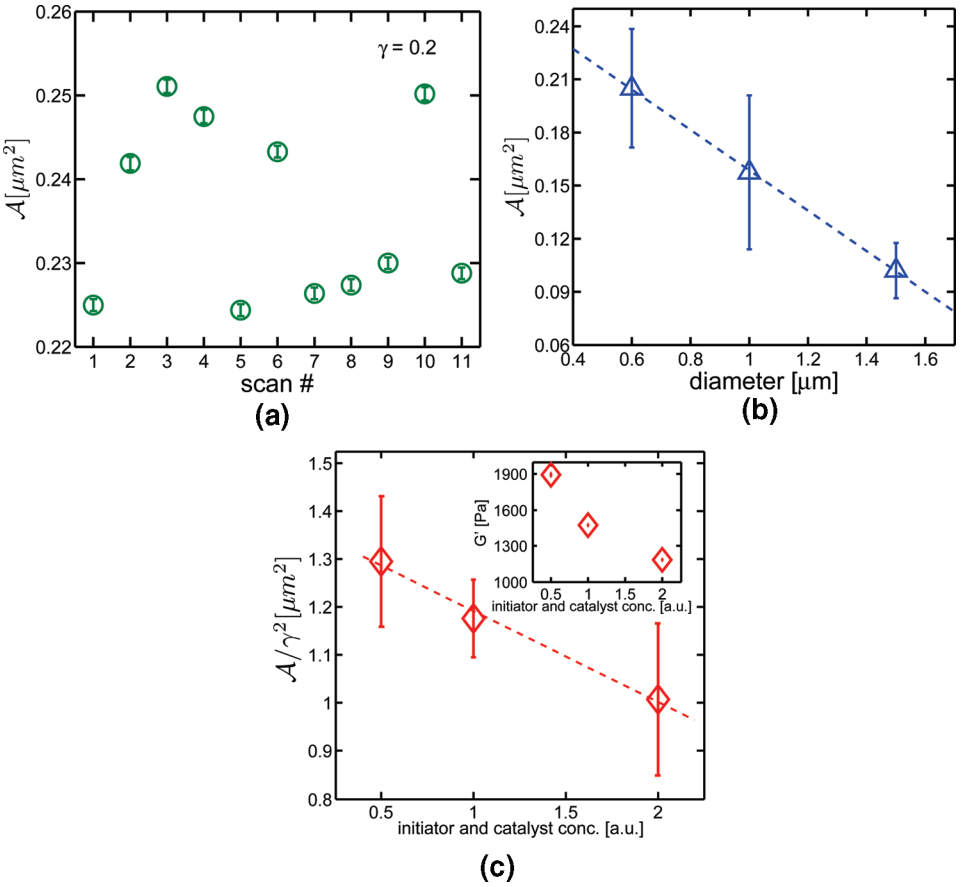

Figure 5. (a) Nonaffine parameter, $\mathcal{A}$, in a sample PA gel (7.5% acrylamide and 0.06% bis), sheared repeatedly under $\gamma = 0.2$ strain. (b) Average nonaffine parameter in a sample PA gel measured using fluorescent tracer beads of average diameters of 600 nm, 1 μm, and 1.5 μm. $\mathcal{A}$ decreases with increasing tracer-bead diameter. Measurements shown here were performed on a sample PA gel with 7.5% acrylamide and 0.06% bis, sheared 11 times at a strain of $\gamma = 0.3$. (c) Elastic shear modulus decreases with increasing initiator and catalyst concentrations for PA gel where the monomer and cross-link concentrations have been kept constant (inset). $\mathcal{A}$ decreases linearly with increasing initiator and catalyst concentrations. Data are shown here for a 7.5% acrylamide and 0.03% bis PA gel.

In section 2 of the Supporting Information, we compute the corrections due to the finite size R of the bead in a simplified model of electrostatics in random media, which is a scalar analogue to the elastic problem. In the limit of $R \to 0$ the nonaffine parameter $\mathcal{A}$ smoothly approaches the limit of point probe, while in the limit of $R/\xi \gg 1$, $\mathcal{A}$ approaches a different value which is simply related to the $R \to 0$ value by a constant factor of $O(1)$. This simple calculation is consistent with the experimental observation (Figure 5b) that $\mathcal{A}$ is not very strongly affected by the bead size, R. However, the exact dependence is not captured by the calculation.

4.5. Effects of Initiator and Catalyst Concentration. Finally, we explored the effects of reaction kinetics on the strain-normalized nonaffinity measure, $\mathcal{A}/\gamma^2$. To do that, we prepare PA gels with same amount of monomer and cross-link concentration, viz., 7.5% acrylamide and 0.03% bis, but with the initiator and stabilizer (TEMED and APS, respectively) concentrations twice and half of the normal amount used. The gel reactions proceed faster (slower) as a result, respectively, yielding lower (higher) plateau shear modulus for twice (half) the normal initiator and catalyst concentrations (inset in Figure 5c). The $\mathcal{A}/\gamma^2$ values calculated for these samples are still within range of $1.65 \pm 0.63\ \mu m^2$, the measured average for 7.5% acrylamide PA gels, leading us to believe that measured values of $\mathcal{A}/\gamma^2$ are still dominated by the inhomogeneities in these gels. Error bars reflect the standard deviation in the ensemble-averaged nonaffinity values measured for four scans over each sample volume. Within this prescribed range, though, there is a slight inverse dependence of $\mathcal{A}/\gamma^2$ on the concentration of TEMED and APS (Figure 5c) which we do not understand.

5. CONCLUSIONS

Nonaffine deformations under shear are measured in a simple cross-linked gel and are employed to provide insight about inhomogeneities in flexible polymer gels. Results indicate that, for a wide range of applied strain, γ, the shear modulus remains independent of strain and the nonaffine parameter, $\mathcal{A}$, which is the mean-square nonaffine deviation in the PA gels, is proportional to the square of the strain applied. These results agree with small-strain predictions in ref 2 based on linear elasticity and support the conjecture that $\mathcal{A}$ scales as γ^2 as long as the shear modulus remains independent of γ. Interestingly, the magnitude of $\mathcal{A}$ is greater than what one would expect from theoretical calculations assuming that the PA gels are nearly ideal and the only source of disorder is from the frozen-in thermal fluctuations at gelation. Furthermore, the degree of nonaffinity appears to be independent of polymer chain density and cross-link

concentration. Thus, we posit that there are additional built-in inhomogeneities in the PA gels that lead to the large nonaffininity we observe. Indeed, there is ample evidence in the existing literature of the presence of such inhomogeneities in PA gels due to a difference in the hydrophobicities of the (bis)acrylamide and acrylamide monomers. Combining the inhomogeneity length scale estimated from atomic force microscopy measurements, i.e., $\xi_G \sim 200$ nm, with the nonaffinity measurements, we calculate the magnitude of local variations in elastic modulus, $\delta G'/G'$, to be ~ 7. Our measurements of nonaffinity in PA gels, which are model flexible polymer gels, provide a benchmark for the degree of nonaffinity in soft materials and will serve as an interesting comparison to nonaffinity in more complicated materials such as semiflexible biopolymer networks.

■ ASSOCIATED CONTENT

Supporting Information. Section 1: a detailed derivation of the nonaffine correlation function; section 2: calculates the correction needed to account for the finite size of the tracer beads; section 3: explores the correlations in the nonaffine displacements between tracer bead pairs in a given sample as a function of their separation distance; section 4: an alternative approach in calculating the strain-normalized nonaffine parameter of PA gels. This material is available free of charge via the Internet at http://pubs.acs.org.

■ AUTHOR INFORMATION

Corresponding Author
*E-mail: abasu@sas.upenn.edu.

■ ACKNOWLEDGMENT

This work was supported by the MRSEC DMR-0520020, DMR-0505048, DMR-0079909, and NSF DMR-0804900 grants.

■ REFERENCES

(1) Rubinstein, M.; Panyukov, S. *Macromolecules* **1997**, *30*, 8036–8044.
(2) DiDonna, B. A.; Lubensky, T. C. *Phys. Rev. E* **2005**, *72*, 066619.
(3) Rubinstein, M.; Panyukov, S. *Macromolecules* **2002**, *35*, 6670–6686.
(4) Glatting, G.; Winkler, R. G.; Reineker, P. *Polymer* **1997**, *38*, 4049–4052.
(5) Everaers, R. *Eur. Phys. J. B* **1998**, *4*, 341–350.
(6) Svaneborg, C.; Grest, G. S.; Everaers, R. *Phys. Rev. Lett.* **2004**, *93*, 257801.
(7) Sommer, J. U.; Lay, S. *Macromolecules* **2002**, *35*, 9832–9843.
(8) Head, D. A.; Levine, A. J.; MacKintosh, F. C. *Phys. Rev. Lett.* **2003**, *91*, 108102.
(9) Head, D. A.; MacKintosh, F. C.; Levine, A. J. *Phys. Rev. E* **2003**, *68*, 025101(R).
(10) Wilhelm, J.; Frey, E. *Phys. Rev. Lett.* **2003**, *91*, 108103.
(11) Mackintosh, F. C.; Kas, J.; Janmey, P. A. *Phys. Rev. Lett.* **1995**, *75*, 4425–4428.
(12) Tanguy, A.; Wittmer, J. P.; Leonforte, F.; Barrat, J. L. *Phys. Rev.* **2002**, *B 66*, 174205.
(13) Langer, S. A.; Liu, A. J. *J. Phys. Chem. B* **1997**, *101*, 8667–8671.
(14) Rubinstein, M.; Colby, R. *Polymer Physics*; Oxford University Press: New York, 2003.
(15) Wen, Q.; Basu, A.; Winer, J.; Yodh, A.; Janmey, P. *New J. Phys.* **2007**, *9*, 428.
(16) Treloar, L. R. G. *The Physics of Rubber Elasticity*; Clarendon: Oxford, 1975.
(17) Crocker, J.; Grier, D. *J. Colloid Interface Sci.* **1996**, *179*, 298–310.
(18) Gao, Y.; Kilfoil, M. L. *Opt. Express* **2009**, *17*, 4685–4704.
(19) Mao, X.; Goldbart, P. M.; Xing, X.; Zippelius, A. *Phys. Rev. E* **2009**, *80*, 031140.
(20) Liu, J.; Koenderink, G.; Kasza, K.; MacKintosh, F.; Weitz, D. *Phys. Rev. Lett.* **2007**, *98*, 198304.
(21) Huisman, E. M.; Storm, C.; Barkema, G. T. *Phys. Rev. E* **2008**, *78*, 051801.
(22) de Gennes, P. G. *Scaling Concepts in Polymer Physics*; Cornell University Press: Ithaca, NY, 1979.
(23) Hecht, A.; Duplessix, R.; Geissler, E. *Macromolecules* **1985**, *18*, 2167–2173.
(24) Mallam, S.; Horkay, F.; Hecht, A.; Geissler, E. *Macromolecules* **1989**, *22*, 3356–3361.
(25) Yeung, T.; Georges, P. C.; Flanagan, L. A.; Marg, B.; Ortiz, M.; Funaki, M.; Zahir, N.; Ming, W.; Weaver, V.; Janmey, P. A. *Cell Motil. Cytoskeleton* **2005**, *60*, 24–34.
(26) Cohen, Y.; Ramon, O.; Kopelman, I. J.; Mizrahi, S. *J. Polym. Sci., Polym. Phys. Ed.* **1992**, *30*, 1055–1067.
(27) Bastide, J.; Mendes, E., Jr.; Boue, F.; Buzier, M.; Linder, P. *Makromol. Chem., Macromol. Symp.* **1990**, *40*, 81–99.
(28) Richards, E. G.; Temple, C. J. *Nature* **1971**, *230*, 92–96.
(29) Hsu, T.; Cohen, C. *Polymer* **1984**, *25*, 1419–1423.
(30) Hsu, T.; Ma, D. S.; Cohen, C. *Polymer* **1983**, *24*, 1273–1278.
(31) Lopatin, V. V.; Askadskii, A. A.; Peregudov, A. S.; Vasil'ev, V. G. *J. Appl. Polym. Sci.* **2005**, *96*, 1043–1058.
(32) Weiss, N.; Silberberg, A. *Br. Polym. J.* **1977**, *9* (2), 144–150.
(33) Weiss, N.; Vliet, T. V.; Silberberg, A. *J. Polym. Sci., Polym. Phys. Ed.* **1979**, *17*, 2229–2240.
(34) Pekcan, O.; Kara, S. *Polym. Int.* **2003**, *52*, 676–684.
(35) Lindemann, B.; Schroder, U. P.; Oppermann, W. *Macromolecules* **1997**, *30*, 4073–4077.
(36) Baselga, J.; HernPndez-Fuentes, I.; PiBrola, I. F.; Llorente, M. A. *Macromolecules* **1987**, *20*, 3060–3065.
(37) Nossal, R. *Macromolecules* **1985**, *18*, 49–54.
(38) Kizilay, M. Y.; Okay, O. *Macromolecules* **2003**, *36*, 6856–6862.
(39) Solubility of bis in water = 0.01−0.1 g/100 mL at 18 °C. Solubility of acrylamide in water = 216 g/100 mL.
(40) Wen, Q.; Janmey, P. (manuscript in preparation): An atomic force microscope (DAFM, Veeco, Woodbury, NY) with a sharp conical tip is used to perform nanoindentation on a polyacrylamide gel made of 7.5% acrylamide and 0.1% bis. Working at the "force volume" mode, the AFM scans an area of 1 μm × 1 μm area with a resolution of 16 pixels/mm. At each pixel, a force−indentation curve is obtained and fit to the Hertz model to get the local Young's modulus. Thus, a map of Young's moduli is obtained for a 1 mm^2 area with a spatial resolution of 62.5 nm. The Young's moduli within the map vary from 3800 to 6300 Pa with a mean of 4800 Pa. The length scale of inhomogeneity is approximately 200 ± 100 nm.
(41) Chen, D. T.; Weeks, E. R.; Crocker, J. C.; Islam, M. F.; Verma, R.; Gruber, J.; Levine, A. J.; Lubensky, T. C.; Yodh, A. G. *Phys. Rev. Lett.* **2003**, *90*, 108301.
(42) Starrs, L.; Bartlett, P. *Faraday Discuss* **2003**, *123*, 323–334.
(43) Onck, P. R.; Koeman, T.; van Dillen, T.; van der Giessen, E. *Phys. Rev. Lett.* **2005**, *95*, 178102.
(44) Huisman, E. M.; van Dillen, T.; Onck, P. R.; Van der Giessen, E. *Phys. Rev. Lett.* **2007**, *99*, 208103.